Bioactive Materials 16 (2022) 1–11

Contents lists available at ScienceDirect

Bioactive Materials

journal homepage: www.keaipublishing.com/en/journals/bioactive-materials

Polymersome-mediated cytosolic delivery of cyclic dinucleotide STING agonist enhances tumor immunotherapy

Huan Zheng [a], Beibei Guo [a], Xinyun Qiu [a], Yifeng Xia [a], Yan Qu [a], Liang Cheng [b,***], Fenghua Meng [a,**], Zhiyuan Zhong [a,b,*]

[a] Biomedical Polymers Laboratory, College of Chemistry, Chemical Engineering and Materials Science, and State Key Laboratory of Radiation Medicine and Protection, Soochow University, Suzhou, 215123, PR China

[b] Department of Pharmaceutics, College of Pharmaceutical Sciences, Soochow University, Suzhou, 215123, PR China

ARTICLE INFO

Keywords:
Polymersomes
STING agonists
Cyclic dinucleotide
Immunotherapy
Radiotherapy

ABSTRACT

Cyclic dinucleotides (CDNs) as stimulator of interferon genes (STING) agonists capable of inducing strong antitumor innate immune response are highly promising for tumor immunotherapy. The efficacy of these CDNs is, however, reduced greatly by their fast clearance, poor cell uptake and inefficient cytosolic transportation. Here, we report that reduction-responsive biodegradable chimaeric polymersomes (CPs) markedly enhance tumor retention and cytosolic delivery of a synthetic CDN, ADU-S100, and bolster STING pathway activation in the tumor microenvironment and tumor draining lymph nodes, giving significantly better tumor repression and survival of B16F10 melanoma-bearing mice compared with free CDN control. The superiority of CPs-mediated CDN delivery is further verified in combination therapy with low-dose fractionated radiation, which brings about clearly stronger and longer-term immunotherapeutic effects and protection against tumor re-challenge. The development of nano-STING agonists that are able to overcome the delivery barriers of CDNs represents an effective strategy to potentiate cancer immunotherapy.

1. Introduction

Immunotherapy has turned out to be an attractive way to cure cancer or defer tumor evolution, characterizing long-term effects [1–3]. In recent years, immune checkpoint blocking (ICB) therapy using CTLA-4 antibodies [4,5], PD-1 antibodies [6–8] or PD-L1 antibodies [9,10] has been approved for the treatment of melanoma, lung cancer, and liver cancer. However, the response rate is only about 20% [11–15]. Many researchers have focused on further improving ICB therapy by combining chemotherapy drugs, stereotactic radiosurgery or other immune checkpoint inhibitors [16–19]. Recently, much attention has focused on stimulator of interferon genes (STING), which is the major innate immune pathway involved in the generation of spontaneous antitumor T cell response. The activation of STING pathway by STING agonists, such as cyclic dinucleotides (CDN) including c-diGMP, c-diAMP, and cGAMP, drives the production of type I IFN and other cytokines, and stimulates the maturation of dendritic cells (DCs) and cross-presentation of tumor antigens for subsequent T cell priming [20,21], leading to effective anti-cancer therapy via intratumoral (i.t.) injection [22–24]. A synthetic CDN, ADU-S100, combining with PD-1 antibody has moved to clinical trials in patients with triple-negative breast cancer or relapsed/refractory melanoma. CDNs activate STING pathway by binding to STING protein on endoplasmic reticulum (ER). However, CDNs are anionic and hydrophilic, which renders fast clearance following intratumoral injection and poor internalization by antigen presenting celles (APCs), leading to low bioavailability and reduced efficacy [25].

Local delivery and nanodelivery systems have been investigated to improve the performance of STING agonist CDNs [26]. Hartgerink et al. reported that STINGel implanted subcutaneously could sustain CDN release and achieve enhanced cancer immunotherapy in murine oral tumor model [27], though cell entry problem was still not addressed.

Peer review under responsibility of KeAi Communications Co., Ltd.

* Corresponding author. Biomedical Polymers Laboratory, College of Chemistry, Chemical Engineering and Materials Science, and State Key Laboratory of Radiation Medicine and Protection, Soochow University, Suzhou, 215123, PR China.

** Corresponding author.

*** Corresponding author.

E-mail addresses: chengliang1983@suda.edu.cn (L. Cheng), fhmeng@suda.edu.cn (F. Meng), zyzhong@suda.edu.cn (Z. Zhong).

https://doi.org/10.1016/j.bioactmat.2022.02.029
Received 28 October 2021; Received in revised form 15 February 2022; Accepted 22 February 2022
Available online 4 March 2022

Murine tumors were greatly suppressed via a single *i.t.* administration of STINGel [28] or CDN-loaded PLGA microparticles [29]. Liu et al. found that cationic silica nanoparticles with excellent stability and high CDN loading elicited strong local inflammation and tumor cell death [30]. In particular, liposomes and polymersomes are of interest to improve intracellular CDN delivery. For instance, cationic liposomes loading CDN via electrostatic interaction have shown to enhance cytosolic delivery of CDNs [31,32]. Wilson et al. reported that pH-sensitive polymersomes could chaperone cGAMP into tumor cells and greatly enhance STING activation and therapeutic activity via *i.t.* or *i.v.* administration [33,34]. Given STING agonists taking effect in the cytosols, robust and cytoplasmic environment-responsive biodegradable nanocarriers would likely be more preferable for CDN delivery.

Herein, we report that a CDN STING agonist, ADU-S100, formulated with reduction-responsive biodegradable chimaeric polymersomes (CPs) markedly enhances its tumor retention and cytosolic delivery, boosting STING pathway activation and antitumor immunotherapy of malignant melanoma in mice (Fig. 1a). CPs decorated with diverse tumor-targeting peptides have been previously shown to mediate efficient RNAi and protein therapy of non-small cell lung cancer and glioblastoma [35–37]. Unlike siRNAs and proteins, CDNs are small molecular weight drug but with rigid structure and highly hydrophilic nature, which makes most delivery systems inapplicable. Interestingly, CPs demonstrated not only a high and stable loading of ADU-S100 but also enhanced cytosolic release of ADU-S100 into DCs, which was shown to significantly boost immunotherapy and furthermore radioimmunotherapy when combining with fractionated low dose X-ray irradiation. Radiotherapy (RT) as a critical and auxiliary antitumor therapy can release tumor-associated antigens and enhance cytoplasmic DNA sensing through cGAS/STING pathway to induce type I IFN production, thereby promoting DC maturation and T cell activation, leading to innate and adaptive immune responses [38–40]. However, high doses of RT may cause systemic toxicity, while low doses are generally not sufficient to eliminate tumors. Moreover, RT induced STING activation is transient, thus the anti-tumor effect is temporary [41]. The combination of CPs-CDN and fractionated low-dose RT would likely induce strong and durable radioimmunotherapy while cause little systemic toxicity.

2. Materials and methods

2.1. Preparation and characterizations of CDN loaded polymersomes (CPs-CDN)

Poly(ethylene glycol)-b-poly(dithiolane trimethylene carbonate-co-trimethylene carbonate)-b-polyethyleneimine copolymer (PEG-P(TMC-DTC)-PEI, M_n = 5-(15.5–2.1)-0.6 kg/mol) dissolved in 100 μL dimethylformamide (DMF) (10 mg/mL) was slowly added to 900 μL HEPES buffer (5 mM, pH 6.8) containing 0.16 mg CDN or a Cy3-labeled linear dinucleotide (Cy3-diAMP). After stirring for 10 min, the mixture was dialyzed against HEPES (MWCO 3500 Da) for 3 h and then against PB (10 mM, pH 7.4) for 30 min. The preparation of empty CPs was the same except no CDN in the buffer. The morphology of CPs was characterized by transmission electron microscopy (TEM). To prepare Cy3-diAMP loaded Cy5-labeled polymersomes (Cy5-CPs-Cy3-diAMP) for *in vivo* imaging, Cy5 labeled polymer Cy5-PEG-P(TMC-DTC) and PEG-P(TMC-DTC) (w/w, 1/50) in 50 μL DMF (10 mg/mL) was slowly added to 450 μL HEPES buffer (5 mM, pH 6.8) containing 0.08 mg Cy3-diAMP. Cy3-diAMP was used as a model for CDN because it is technically difficult to obtain Cy3-labeled CDN. While diAMP has similar molecular weight and chemical composition as CDN. The CPs showed similar loading efficiency for diAMP and CDN and the resulting formulations had almost the same size and size distribution. CPs-diAMP have comparable features to CPs-CDN.

The size and zeta potential of polymersomes were measured by Zetasizer Nano-ZS instrument. The stability of the CPs-CDN was studied by tracking size changes after 3-week storage or incubation in PBS containing 10% FBS for 48 h (pH 7.4, 37 °C). The encapsulation efficiency of CDNs was determined by NanoDrop 2000 at 260 nm.

In vitro release was studied using Cy3-diAMP as a model CDN. CPs-Cy3-diAMP prepared as above was transferred into dialysis tubes (MWCO 140 kDa) and dialyzed against 20 mL PB (10 mM, pH 7.4) with or without 10 mM GSH at 37 °C with mild stirring. At preset intervals, 5 mL medium was taken out to quantify the released dinucleotide by fluorometry (n = 3) and 5 mL fresh medium was supplemented.

2.2. The endocytosis and endosomal escape behavior of CPs-CDN in BMDCs

The cellular uptake of CPs-CDN was studied in bone marrow derived dendritic cells (BMDC), bone marrow derived macrophages (BMDM), B16F10 and L929 cells using Cy5 labeled CPs-CDN. In brief, into BMDC (1×10^5 cells/well), BMDM (1×10^5 cells/well), B16F10 (5×10^5 cells/well), or L929 cells (5×10^5 cells/well) in 6-well plates, were added 200 μL Cy5 labeled CPs-CDN (Cy5: 3.2 nM). After 4 h incubation at 37 °C, the cells were trypsinized, centrifuged (1000 rpm, 5 min), washed with PBS and analyzed by flow cytometry.

To study the endosomal escape behavior, BMDCs were cultured in 24-well plate (2×10^5 cells/well) for 24 h. 100 μL CPs-Cy3-diAMP or free Cy3-diAMP (300 nM Cy3 in PB) was added and incubated for 4 h at 37 °C. The culture medium was removed and Lysotracker-deep-red (100 nM) was added to stain endosomes/lysosomes for 1 h. The cells were then fixed with 4% paraformaldehyde for 15 min and washed with PBS, and stained with DAPI for 5 min. The fluorescence images were obtained by using confocal laser scanning microscope (CLSM).

2.3. The maturation, cytokine secretion and protein expression of BMDCs

BMDCs cultured in a 6-well plate (1×10^6 cells/well) were added with CPs-CDN, free CDN (1 μg CDN/mL), empty CPs or PBS. After incubation for 24 h, the cells were treated with mouse antibodies PerCP/Cy5.5-αCD45, FITC-αCD11c, APC-αCD80, and PE-αCD86 for analysis of DC maturation using flowcytometry. The culture medium was collected and centrifuged (3000 rpm, 10 min), and the concentrations of IFN-β and TNF-α were measured with mouse IFN-β and TNF-α ELISA kits.

For Western blot assays, BMDCs cultured in 6-well plate (2×10^6 cells/well) were treated with CPs-CDN, free CDN (200 μL, 1 μg CDN/mL) or PBS for 6 h, and then washed, digested, and lysed using standard procedure before adding antirabbit pIRF3 (1:1000), pTBK1 (1:1000) or GAPDH (1:1000) antibodies followed by secondary antibody goat antirabbit IgG (1:2000) (supporting information).

2.4. Tumor retention of CPs -CDN after i.t. injection

All animal experiments were approved by the Animal Care and Use Committee of Soochow University and all protocols conformed to the Guide for the Care and Use of Laboratory Animals. For establishing B16F10 tumor-bearing mouse model, 1.5×10^5 B16F10 cells in 50 μL PBS containing 40% Matrigel were injected into the right flank of 6-week-old C57BL/6J mice (ca. 20 g). At tumor volume of ~150 mm^3, free Cy3-diAMP (Cy3: 0.2 μg/mouse) or Cy5-labeled CPs-Cy3-diAMP (Cy3: 0.2 μg/mouse, Cy5: 0.2 μg/mouse) in 50 μL PBS were intratumorally (i.t.) injected. After 24 h, tumors were isolated, and tumor slices were imaged using CLSM to visualize the distribution of Cy3-diAMP and Cy5-labeled CPs in tumor.

2.5. Plasma concentration of CDN after i.t. injection

Cy7-labeled AMP (Cy7-AMP) was used as a CDN model to study the blood concentration of CDNs upon i.t. injection. To mice bearing B16F10 tumors (tumor volume of ~100 mm^3), 50 μL free Cy7-AMP or CPs-Cy7-AMP (10 μg Cy7/mouse) was i.t. injected. At preset time points, 70 μL

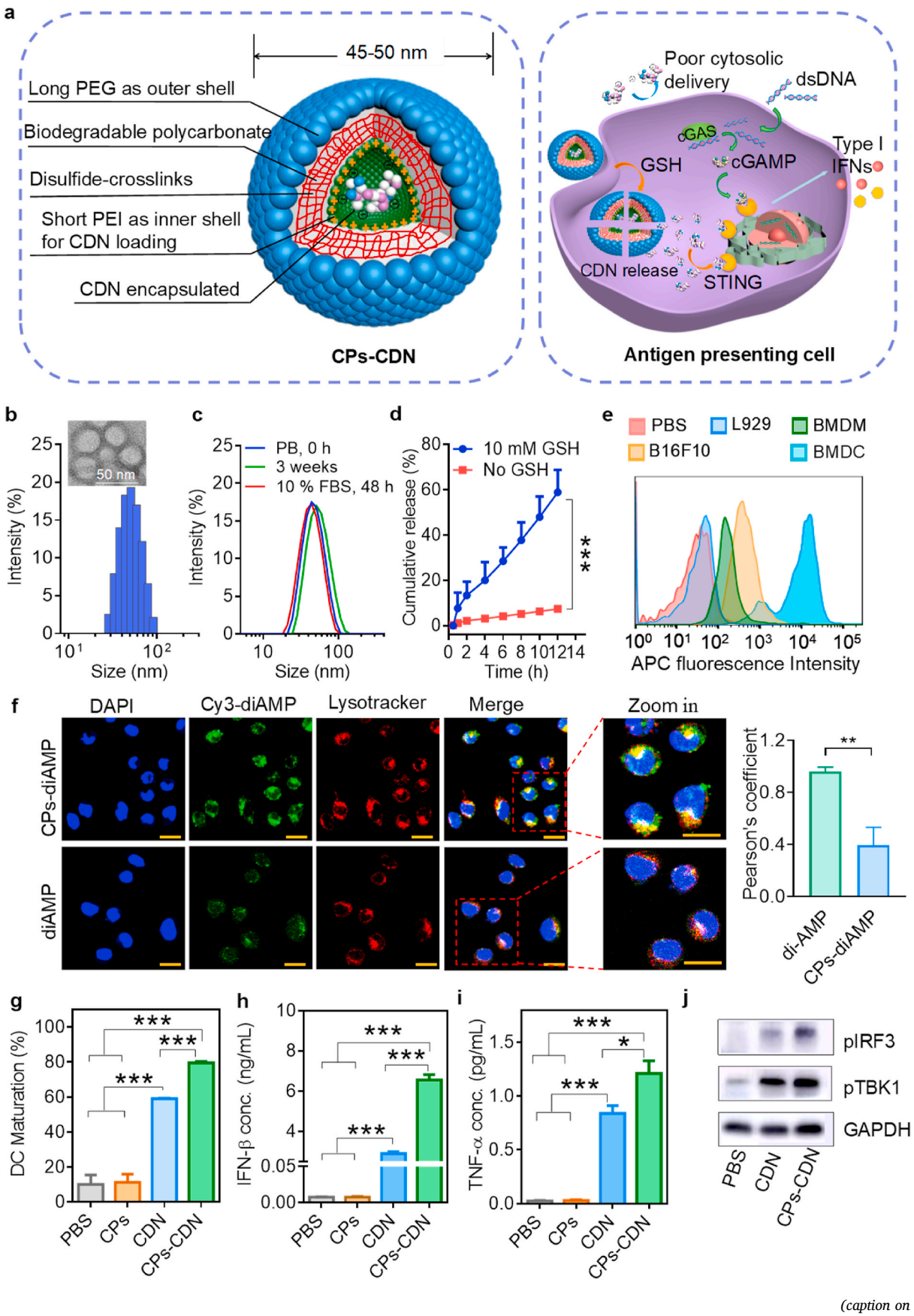

(caption on next page)

Fig. 1. Design and characterizations of CPs-CDN. **a** Schematic illustration of CPs-CDN and CP-mediated cytoplasmic release of CDN. **b** Size distribution of CPs determined by DLS. Inset: TEM image. **c** Size distribution profiles of CPs-CDN, after 3-week storage or in buffer containing 10% FBS for 48 h (pH 7.4, 37 °C). **d** *In vitro* Cy3-diAMP release from CPs in the presence or absence of 10 mM GSH at 37 °C (concentration: 100 μg/mL, n = 3). **e** Cellular uptake of Cy5 labeled CPs-CDN by BMDC, BMDM, B16F10, and L929 fibroblasts using flowcytometry. **f** CLSM images of BMDCs incubated with CPs-Cy3-diAMP or Cy3-diAMP (green) for 4 h and calculation of Pearson's coefficient. The nuclei and lysosomes/endosomes were stained with DAPI (blue) and Lysotracker deep red (red), respectively. Scale bars: 20 μm **g** FACS determination of BMDC maturation ($CD80^+CD86^+$) after 24 h incubation with PBS, CPs, CDN or CPs-CDN (n = 3). ELISA detection of IFN-β (**h**) and TNF-α (**i**) in cell culture medium (n = 3). **j** Western blot measurements of pTBK1 and pIRF-3 expression. Statistical analysis: one-way ANOVA with Tukey multiple comparisons. *p < 0.05, **p < 0.01, ***p < 0.001. (For interpretation of the references to colour in this figure legend, the reader is referred to the Web version of this article.)

blood was withdrawn from ophthalmic vein of mice into heparinized tubes, and immediately centrifuged at 5000 rpm for 5 min. 20 μL plasma was taken and incubated at 37 °C overnight with 180 μL acetonitrile/H_2O (1:1, v/v) containing dithiothreitol (DTT, 20 mM) to extract Cy7-AMP. After centrifugation (15000 rpm, 20 min), Cy7 concentration in the plasma was quantified using a microplate reader (Thermo, USA).

2.6. Antitumor therapy in mice bearing B16F10 tumor

To investigate the anti-tumor effect of CPs-CDN, the mice bearing B16F10 tumors (tumor volume of ~50 mm^3) were i.t. injected with 50 μL CPs-CDN or free CDN (at 1.0 mg CDN/kg) on day 0, 3, and 7 using PBS as a control (n = 7). Tumor volume, body weight and survival rate of the mice were recorded. Body weight and tumor size were measured every two days, and relative to their initial values on day 0. Tumor volume was calculated from the formula: $V = L*W^2/2$ (L and W are tumor length and width, respectively). Mice were designated dead when the mice died, body weight loss was over 15%, or tumor volume was over 2000 mm^3.

To investigate the anti-tumor effect of local fractionated X-ray combined with CPs-CDN, the mice bearing B16F10 tumors (~50 mm^3) were locally radiated with 3 Gy or 5 Gy X-ray on day 0, 3, and 6, followed by *i.t.* injection of 50 μL CPs-CDN (0.5, 1.0 or 1.5 mg CDN/kg), CDN (1.0 mg/kg), empty CPs or PBS on day 1, 4 and 8 (n = 7).

The cured mice were re-challenged with secondary tumors by subcutaneous injection of 1.5×10^5 B16F10 cells into the left flank on day 176 post initial tumor inoculation using healthy mice as control. Tumor volume was monitored every two days without any additional treatment.

2.7. Analysis of the immune cells and cytokines

The mice bearing B16F10 tumors (~100 mm^3) were locally radiated with 3 Gy or 5 Gy X-ray on day 0, 3, and 6, and i.t. injected with 50 μL CPs-CDN, CDN (1.0 mg CDN/kg) or PBS on day 1, 4 and 8 (n = 4). At 6 h after last administration, the mouse blood was collected and plasma concentrations of IFN-β and TNF-α were measured with mouse IFN-β and TNF-α ELISA kits.

At 48 h after last administration, the mice were sacrificed and the tumors and tumor draining lymph nodes (TDLN) were harvested to obtain single cell suspensions in PBS containing 1% FBS. The cells were treated with ACK buffer for 10 min at 4 °C to lyse red blood cells, then stained with corresponding antibodies at 4 °C for 20 min in the dark (10^6 cells/tube). To prevent cell sinking to the bottom, cell suspensions were gently tapped every 5 min. Mouse antibodies PerCP/Cy5.5-αCD45, FITC-αCD11c, APC-αCD80, and PE-αCD86 were used for DC maturation analysis. Mouse antibodies PerCP-αCD45, FITC-αCD11b and APC-αCD206 were used for macrophage phenotype analysis. Mouse antibody APC-αCD3, FITC-αCD8α and PE-αCD4 were used for $CD8^+$ T and $CD4^+$ T cell labeling. The cells were washed twice with PBS containing 1% FBS before evaluation using flow cytometer.

To study hematoxylin and eosin (H&E) staining and immunohistochemistry, at 48 h after last administration one mouse from each group was randomly selected. Tumors and major organs (heart, liver, spleen, lung, kidney) were excised, washed, fixed, embedded, sectioned (5 μm) and stained with H&E for pathological analysis. For immunohistochemical staining of tumor slices, paraffin sections (5 μm) were immuno-stained with rabbit αCD8 (1:500; Abcam) or rabbit αCRT antibody (1:200; Abcam) for 1 h at 37 °C, followed with Alexa Fluor 633-conjugated goat anti-rabbit secondary antibody (1:500; Invitrogen). The nuclei were finally stained with DAPI, and fluorescence images were taken by using a fluorescence microscope (Olympus BX41).

2.8. Statistical analysis

Data were presented as the mean ± standard deviation and analyzed using GraphPad Prism. Significant differences among groups were determined by one-way ANOVA with Tukey multiple comparison tests, and the survival rate was analyzed by Kaplan-Meier technique with a log-rank test for comparison. $*p < 0.05$ was considered significant, and $**p < 0.01$, $***p < 0.001$ were considered highly significant.

3. Results and discussion

3.1. Preparation of CPs-CDN

CDNs are water-soluble, small and rigid molecules which renders few nanosystems capable of efficiently loading and delivering them to DCs [42,43]. Here, we investigated chimaeric polymersomes (CPs) based on PEG-P(TMC-DTC)-PEI copolymer, which has shown to mediate efficient RNAi therapy of solid tumors [44], as a tool for cytoplasmic delivery of ADU-S100, a CDN STING agonist under clinical trial. PEG-P(TMC-DTC)-PEI was synthesized with an M_n of 5.0-(15.5–2.1)-0.6 kg/mol (^{1}H NMR shown in Fig. S1), from which CPs self-assembled exhibited a unimodal size distribution profile with a hydrodynamic size of 47 nm (Fig. 1b), neutral zeta potential (Table S1), and a spherical and vesicular structure (Fig. 1b). CPs could efficiently load ADU-S100 to afford a CDN loading content of 17.2 wt% (Table S1). The loading efficiency for CDN was 86.0%, which was similar to CPs for siRNA and CpG ODN [37,44,45] and much higher than other nanoparticles and liposomes for CDNs (<45%) [31,34,46]. Notably, CDN-loaded CPs (CPs-CDN) revealed excellent colloidal stability in buffer containing 10% FBS or upon storage for 3 weeks (Fig. 1c). *In vitro* release studies using Cy3-diAMP as a model CDN showed that ca. 7.4% and 58.9% CDN was released from CPs in 12 h under physiological condition and 10 mM glutathione environment, respectively (Fig. 1d), verifying that CPs can stably load CDN while trigger CDN release under cytosolic reductive condition, similar to previous reports for siRNA and protein therapeutics [35–37].

3.2. Cytoplasmic CDN delivery and STING pathway activation

The STING pathway is closely related to the innate immune system, especially the function of antigen-presenting cells (APCs) [32,47,48]. To activate immune response, STING agonist CDNs have to be delivered to APCs and bind with STING proteins located on endoplasmic reticulum. We studied the cellular uptake of CPs-CDN in BMDC, BMDM, B16F10 and L929 cells by flow cytometry using Cy5 labeled CPs-CDN. Fig. 1e shows that at 4 h incubation, BMDCs endocytosed one to three orders of magnitude more CPs-CDN than B16F10, BMDM and L929 fibroblasts, supporting efficient and preferential internalization of CPs-CDN by DCs. To study the intracellular trafficking behavior of CPs-CDN using CLSM,

we stained the endo/lysosomes with lysotracker. Fig. 1f shows that BMDCs after 4 h incubation with CPs-Cy3-diAMP had much stronger Cy3 fluorescence and higher level of separation from endo/lysosomes than free Cy3-diAMP. Pearson's coefficient was calculated to be significantly decreased for CPs-Cy3-diAMP compared to free Cy3-diAMP (**p), confirming an efficient internalization and cytosolic release of CDNs.

By activating STING pathway, CDNs could induce production of type I IFN and promote DC maturation [49], which plays an important role in antigen cross-presentation and T cell priming [50,51]. To investigate STING activation ability of CPs-CDN, we incubated BMDCs with CPs-CDN for 24 h and analyzed DC maturation and cytokine release. Fig. 1g shows that empty CPs did not stimulate DC maturation, although PEI was reported as adjuvant for interferon induction and DC maturation [52,53]. This low DC maturation supports that PEI is located inside the polymersomes. Notably, CPs-CDN increased the proportion of mature BMDCs ($CD80^+CD86^+$) to 80.5%, which was significantly higher than free CDN (59.3%). IFN-β secretion, as a hallmark of STING activation [54], in free CDN group was 410-fold higher than that in CPs and PBS groups, while CPs-CDN further doubled the IFN-β secretion compared with free CDN (***p) (Fig. 1h). CPs-CDN induced also significantly higher TNF-α production than free CDN (Fig. 1i). We further analyzed pTBK1 and pIRF-3 expression, as STING after binding with CDNs will translocate from ER to Golgi and subsequently recruit TANK-binding kinase 1 (TBK1) and activate IFN regulatory factor 3 (IRF3) via a phosphorylation dependent mechanism [55,56]. Fig. 1j reveals that CPs-CDN drastically promoted both pTBK1 and pIRF-3 expression as compared to PBS group and free CDN, further verifying the activation of STING pathway. These results confirm that CPs-CDN can efficiently deliver CDNs to cytosol of BMDCs, leading to enhanced

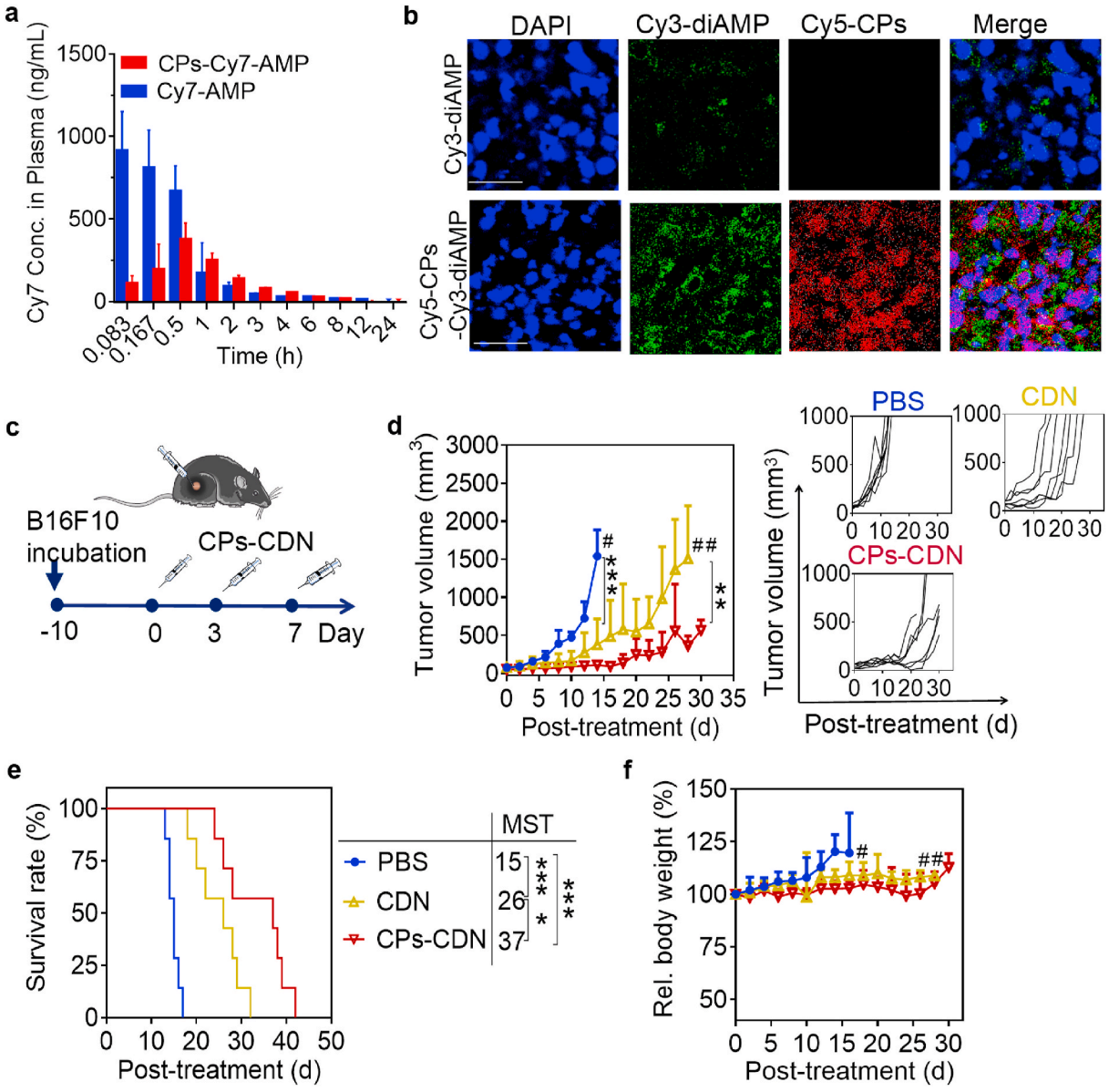

Fig. 2. *In vivo* pharmacokinetics, tumor distribution and antitumor performance of CPs-CDN in B16F10 melanoma-bearing mice. **a** Plasma concentration of Cy7 after a single *i.t.* injection of free Cy7-AMP or CPs-Cy7-AMP (10 μg Cy7/mouse, n = 3). **b** CLSM images of tumor slices at 24 h after single *i.t.* injection of free Cy3-diAMP or Cy5-CPs-Cy3-diAMP. Scale bars: 20 μm **c** Treatment scheme of CPs-CDN against B16F10 melanoma-bearing mice (1 mg CDN/kg). At tumor volume of ca. 50 mm^3, the mice were *i.t.* administered CPs-CDN, CDN, or PBS on day 0, 3 and 7. **d** Tumor growth curves (n = 7) and individual spider plots. **e** Survival rates (n = 7). Kaplan-Meier survival analyses with two-tailed Mantel–Cox tests. **f** Relative body weights (n = 7). Statistical analysis: one-way ANOVA with Tukey's multiple comparisons. Data are represented as mean ± SD. *p < 0.05, **p < 0.01, ***p < 0.001.

activation of STING pathway and production of type I IFNs thus promoting DC maturation.

3.3. Antitumor effect of CPs-CDN

The tumor retention and distribution of CPs-CDN after intratumoral (*i.t.*) administration was investigated in B16F10 melanoma-bearing mice using Cy7-labeled penta-nucleotide (Cy7-AMP) and Cy3-diAMP as CDN models. Fig. 2a shows that free Cy7-AMP quickly diffused into blood circulation from tumor sites yielding a C_{max} in 5 min. In contrast, Cy7-AMP loaded polymersomes, CPs-Cy7-AMP, revealed ca. 10 times lower Cy7-AMP in blood at 5 min and gradually reached C_{max} at 30 min post *i.t.* administration. CPs-Cy7-AMP had over 2 times lower AUC than free Cy7-AMP, supporting that CPs-CDN hinders CDN leakage from the injection site. Free CDNs, even clinically investigating CDNs, suffer from suboptimal cell uptake and bioavailability [33]. To study tumor retention, CLSM images of tumor slices acquired at 24 h post *i.t.* injection of Cy3-diAMP loaded Cy5-labeled CPs exposed strong and widespread Cy3 and Cy5 fluorescence (Fig. 2b). The merged images showed partial separation of Cy3-diAMP (green) from Cy5-labeled CPs (red). In contrast, weak Cy3 fluorescence was seen in tumor slices from free Cy3-diAMP group. The rapid tumor diffusion and extended tumor retention of CPs-CDN is likely due to its optimal particle size of ca. 50 nm. It was reported that small particles of 20–50 nm could penetrate deep into tumor while nanoparticles of less than 20 nm would be quickly cleared from the body [57,58]. These results concluded that CPs-CDN not only prolongs tumor retention and restrains diffusion into blood, but also possibly enhances CDN delivery to tumor infiltrating immune cells as well as tumor cells *in vivo*. Barber et al. reported that dying tumor cells that contain STING agonists could also induce effective STING signaling activation in engulfing immune cells like macrophages to trigger immune response, antigens cross-presentation and CTLs generation [59].

The immunotherapeutic effect of CPs-CDN was investigated using ADU-S100 as a therapeutic CDN model in B16F10 melanoma-bearing mice. When tumor volume reached 50 mm^3, the mice were *i.t.* administered with CPs-CDN, free CDN, or PBS on day 0, 3 and 7 (Fig. 2c). The results displayed clearly that CPs-CDN induced significantly better tumor inhibition than free CDN though free CDN also effectively retarded tumor growth (Fig. 2d). Notably, the median survival time (MST) of CPs-CDN group was extended to 37 d, which was significantly longer than free CDN and PBS groups (26 and 15 d, respectively) (Fig. 2e). Unlike PBS group which showed rapid increase of body weight in 15 d due to aggressive tumor growth, CPs-CDN group had little increase in body weight within 25 d (Fig. 2f). H&E analyses further displayed no tissue damage and infiltration of inflammatory cells to main organs (Fig. S2). The typical toxicity associated with STING pathway is cytokine storm and will cause systemic inflammatory response in the host, multiple tissue and organ damage, or even death, which were all not seen during CPs-CDN treatment. These results indicate that CPs-CDN elicits potent immunotherapy of melanoma without inducing adverse effects.

3.4. Combination of CPs-CDN with X-ray for melanoma radioimmunotherapy

X-ray radiotherapy (RT) as a critical and auxiliary antitumor therapy is widely used in treating patients [60]. The anti-tumor responses elicited by RT mainly include DNA damage, damage-associated molecular patterns (DAMPs) release, and cGAS/STING activation, leading to innate and adaptive immune response [38–40]. The activation of STING pathway is, however, transient, resulting in temporary anti-tumor effect [41]. Herein, we investigated the combination of CPs-CDN and fractionated low-dose X-ray irradiation for strong and durable radioimmunotherapy of B16F10 melanoma (Fig. 3a). When tumor volume reached 50 mm^3, tumors were irradiated with 3 Gy X-ray on day 0, 3 and 6, followed by *i.t.* administration of CPs-CDN, free CDN, empty CPs or PBS on day 1, 4 and 8 (CDN: 20 μg/mouse). The results showed that 3 Gy

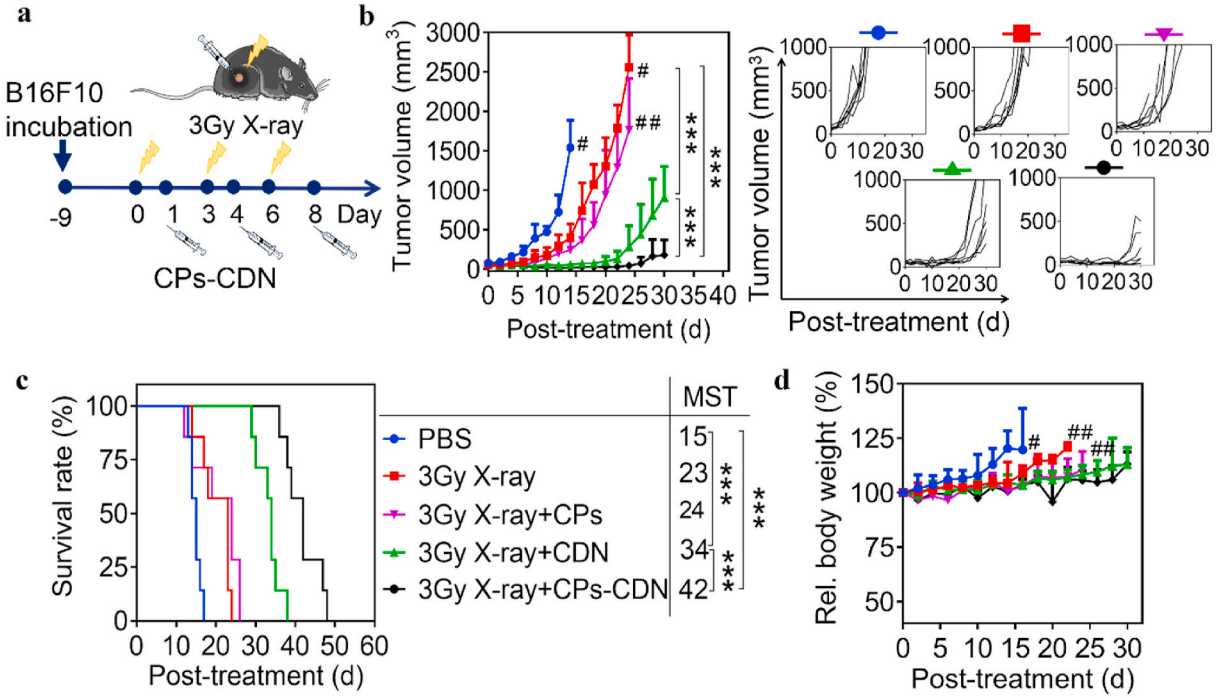

Fig. 3. The combination of CPs-CDN (1 mg CDN/kg) and 3 Gy X-ray for radioimmunotherapy of B16F10 melanoma-bearing mice (n = 7). **a** Tumor inoculation and treatment scheme. When tumor volume reached 50 mm^3, mice were treated by irradiating the tumors with X-ray (3 Gy) on day 0, 3 and 6 followed by *i.t.* administration of CPs-CDN, CDN, CPs or PBS on day 1, 4, and 8. **b** Tumor growth curves and individual spider plots. **c** Survival rates. Kaplan–Meier survival analysis (two-tailed Mantel–Cox test). **d** Relative body weights. Statistical analysis: one-way ANOVA with Tukey's multiple comparisons. Data are represented as mean ± SD. *p < 0.05, **p < 0.01, ***p < 0.001.

X-ray alone or combined with empty CPs could induce inhibition of B16F10 tumor growth to a low extent, and tumors grew exponentially after stopping X-ray irradiation (Fig. 3b). The combination of 3 Gy X-ray with CPs-CDN or free CDN greatly improved the inhibition of melanoma growth, in which CPs-CDN was significantly more potent than free CDN (***p). Accordingly, 3 Gy X-ray + CPs-CDN group brought about the best survival benefit with an MST of 42 d, which was significantly longer than 3 Gy X-ray + free CDN and CPs-CDN groups (Fig. 3c). It is noticed that treatment with 3 Gy X-ray + CPs-CDN at CDN dose of 20 μg/mouse was much better than combo groups at CDN dose of 10 or 30 μg/mouse (Fig. S3). Of note, 3 Gy X-ray alone had only limited improvement of MST over PBS (23 vs 15 d). The group of 3 Gy X-ray + CPs-CDN showed less body weight increase than other groups in 25 d (Fig. 3d), supporting its high potency and low adverse effects.

We further studied the efficacy of radioimmunotherapy of melanoma at a higher X-ray dose of 5 Gy (Fig. 4a). The results showed that 5 Gy X-ray irradiation had better tumor inhibitory effect than 3 Gy (Fig. 4b). However, the mice survival rate was not significantly improved compared with 3 Gy X-ray (MST = 26 vs 23 d) (Fig. 4c), in line with short-term STING activation and transient anti-tumor immune response [41]. The combination of 5 Gy X-ray with CPs-CDN or free CDN markedly further halted melanoma growth. Remarkably, CPs-CDN gave significant survival benefits compared to free CDN (MST: 54 vs 39 d). Three out of seven mice (3/7) became tumor free for both combo groups over an observed period of 176 d post tumor inoculation (Fig. 4c), supporting that combination of RT and STING agonists can elicit durable and strong immunotherapeutic effects [47,61,62]. Importantly, all treatments were well tolerated (Fig. 4d). The activation of STING pathway plays a crucial role in both immune cells and tumor cells, and can regulate multiple stages in the cancer-immunity cycle and induce spontaneous initiation of anti-tumor $CD8^+$ T cell response [62]. The STING agonists need to be delivered to endoplasmic reticulum where STING locates. The efficient cytoplasmic delivery of CPs-CDN makes it a great system for boosting anti-cancer microenvironment. In comparison, toll-like receptors (TLRs)

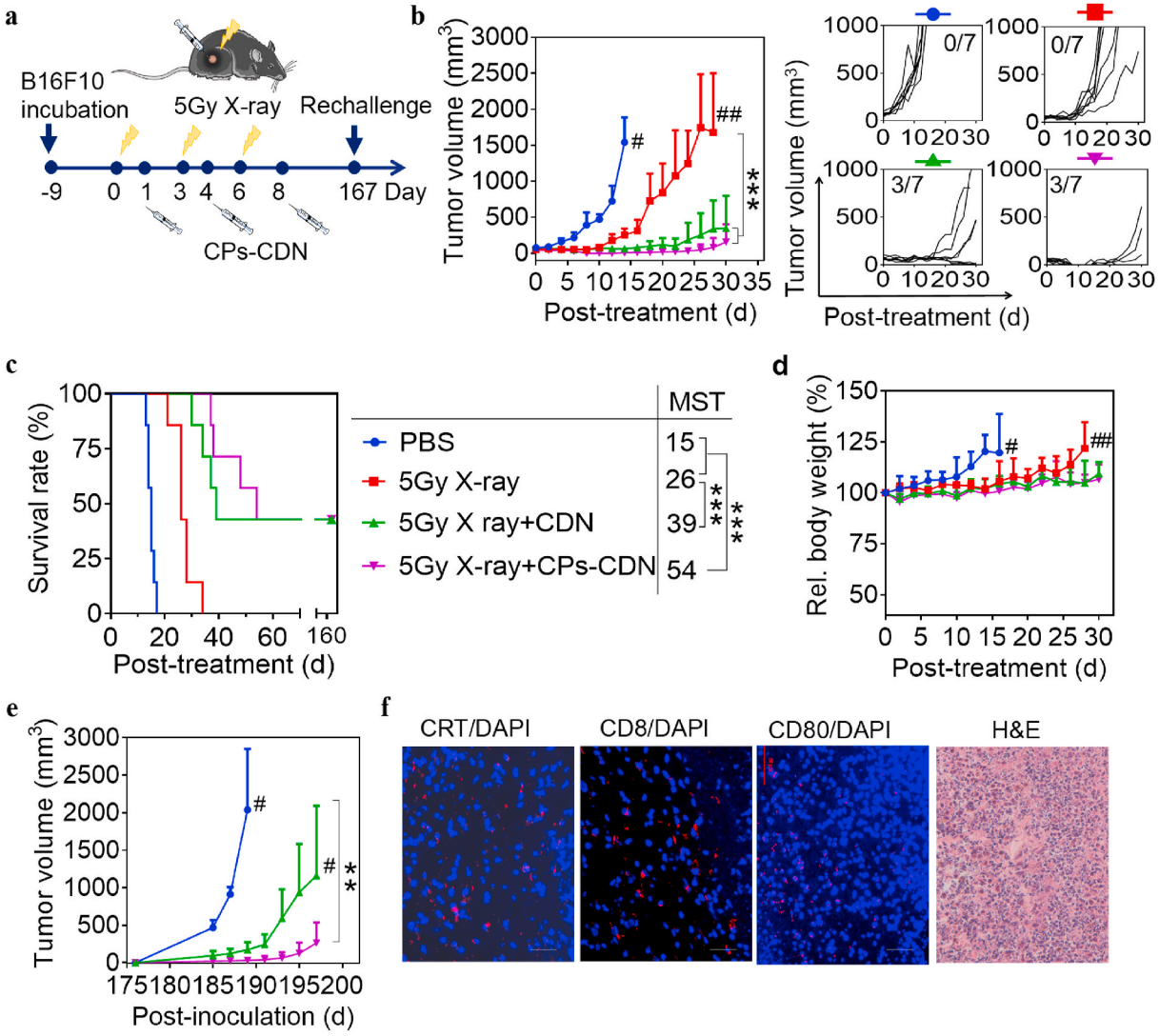

Fig. 4. The combination of CPs-CDN (1 mg CDN/kg) and 5 Gy X-ray for radioimmunotherapy of the mice bearing B16F10 melanoma (n = 7). **a** Tumor inoculation, treatment, and rechallenge scheme. When the tumor volume reached 50 mm^3, the mice were treated by locally irradiating tumors at 5 Gy on day 0, 3 and 6, and *i.t.* administration of CPs-CDN, CDN or PBS on day 1, 4, and 8. **b** Tumor volume and spider plots of individual tumor growth curves (n = 7). **c** Survival rates. Kaplan–Meier analysis (two-tailed Mantel–Cox test). **d** Relative body weights. Statistical analysis: one-way ANOVA with Tukey's multiple comparisons. **e** The cured mice were rechallenged with B16F10 cells on the opposite side on 175 d after the first inoculation (n = 3). **f** Analysis of tumor sections of 5 Gy X-ray + CPs-CDN group. From left to right: immunofluorescence staining of CRT, $CD8^+$ T cells, $CD80^+$ DCs and H&E staining images. Scale bar: 50 μm. For b-e, blue symbols and lines: PBS, red: 5 Gy X-ray, green: 5 Gy X-ray + CDN, purple: 5 Gy X-ray + CPs-CDN. *p < 0.05, **p < 0.01, ***p < 0.001. (For interpretation of the references to colour in this figure legend, the reader is referred to the Web version of this article.)

are pattern recognition receptors (PRRs) of the innate immune system, and the delivery of agonists of intracellular TLRs such as such as TLR3/7/8/9 need to be released in endosomes/lysosomes.

The cured mice were further re-challenged with subcutaneous inoculation of 1.5×10^5 B16F10 cells at the opposite flank on day 176. The results demonstrated that one mouse from 5 Gy X-ray + CPs-CDN group rejected tumor, while the other two mice exhibited greatly retarded tumor growth as compared with PBS group (Fig. 4e). The mice from 5 Gy X-ray + CDN group also revealed delayed tumor growth compared with PBS group; nevertheless, all three mice re-grew tumors and died in 23 d after tumor rechallenge. The immunofluorescence staining of tumor slices of 5 Gy X-ray + CPs-CDN group displayed extensive tumor cell necrosis, tremendous calreticulin (CRT) exposure, $CD80^+$ DCs and $CD8^+$ T cell infiltration (Fig. 4f, Fig. S4), in agreement with RT triggered DNA damage and release of DAMPs (CRT) as tumor associated antigens (TAA) that serve as "eat-me" signal for maturation of APCs and enhancing tumor-specific T cell response [38–40]. These results confirm that radioimmunotherapy with 5 Gy X-ray + CPs-CDN induces strong and durable adaptive immune response.

3.5. Radioimmunotherapy with CPs-CDN and X-ray promotes pro-inflammatory TME

The successful immunotherapy depends not only on the activation of APCs but also on the effective elimination of the immunosuppressive TME, which largely counteracts the anti-tumor immunity [34]. Here, we evaluated the effect of CPs-CDN and its combination with X-ray on immune microenvironment of B16F10 melanoma. Giving that DCs are the major immune cells in activation of STING pathway, DC maturation in the tumor draining lymph node (TDLN) at 48 h after the last injection was analyzed by flow cytometry. TDLN plays a major role in accommodating mature DCs that present antigen information to specific T cells. The results showed that *i.t.* injection of free CDN stimulated a great increase of mature DCs ($CD11c^+CD80^+CD86^+$) in TDLN than PBS (Fig. 5a), whereas DC maturation in CPs-CDN group was further more significant than free CDN group (67.7% vs. 56.1%, **p), which is consistent with *in vitro* BMDC activation results. The efficient TDLN transportation of CPs-CDN is likely due to its small size (47 nm) and easy access to lymphatic lumen from the interstitial space [63]. While 3 Gy X-ray alone had limited ability to promote DC maturation, its combination with free CDN and in particular CPs-CDN significantly augmented DC maturation. Interestingly, 5 Gy X-ray + CPs-CDN could further improve the proportion of mature DCs in TDLN to 89.9%, which was significantly higher than 3 Gy X-ray + CPs-CDN group (*p) and CPs-CDN group (***p). This could be ascribed to an increased release of ICD and DAMPs (CRT, HMGB1 and ATP) inducing specific activation of effector T cells to inhibit tumor growth [38,39], and to enhanced STING pathway activation caused by 5 Gy X-ray than 3 Gy X-ray [64].

Cytotoxic T lymphocytes (CTLs) are the key effector cells in cancer immunotherapy. The proportions of tumor-infiltrating $CD8^+$ and $CD4^+$ T cells after immunotherapy and combination therapy were studied and analyzed (Fig. 5b, Fig. S5). The gating strategies were shown in Fig. S6. Fig. S5 shows that there were no significant differences in $CD4^+$ T cells among groups. Although stimulating DC maturation, free ADU-S100 did not increase the CTL proportion in TME, nor did 3 Gy X-ray. In sharp contrast, CPs-CDN greatly promoted tumor infiltration of CTLs (*p),

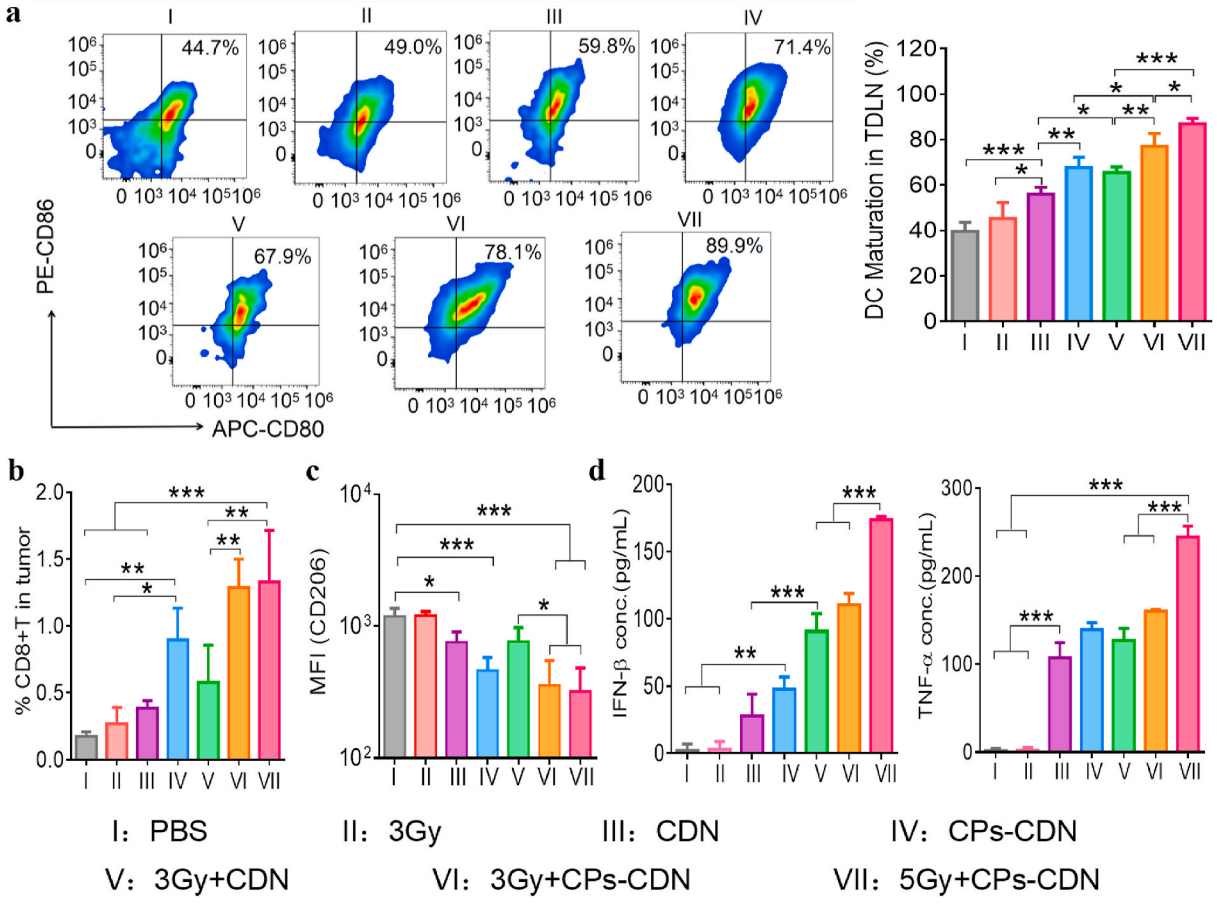

Fig. 5. Anti-tumor immune response induced by the combination of CPs-CDN and X-ray in B16F10-bearing mice (n = 4). **a** Typical histograms and quantitation of DC maturation in TDLN analyzed by FACS. **b** The proportion of $CD8^+$ T cells in tumors (n = 4). **c** The positive expression of CD206 (mean fluorescence intensity of CD206-Alexa Flour 647) on macrophages in TME (n = 4). **a-c**: TDLN or tumors were harvested at 48 h after the last injection. **d** Plasma concentrations of IFN-β and TNF-α of the mice at 6 h after last injection (n = 3). Statistical analysis: one-way ANOVA with Tukey's multiple comparisons. *p < 0.05, **p < 0.01, ***p < 0.001.

showing the benefits of polymersomal formulation in recruiting CTL to TME. The combination of CPs-CDN with X-ray further significantly more increased CTLs than free CDN + X-ray (**p), in accordance with the results of DC maturation. Notably, compared with PBS, a significant reduction of immunosuppressive M2 phenotype macrophages (M2M, CD11b + CD206+) was observed for free CDN (*p) and CPs-CDN (***p) groups (Fig. 5c, Fig. S5). The combination with X-ray with CPs-CDN led to a further decrease of M2M contents. These results indicate that the combination of CPs-CDN with X-ray not only enhances immunostimulatory effects but also alleviates immunosuppressive environment in B16F10 tumors. In this study, total dose of 15 Gy (3 × 5 Gy) was applied in combination with CPs-CDN, inducing strong and durable antitumor efficacy. This dose of radiation is low compared with many previous studies in mouse models. In clinical settings, fractionated RT combination with immunotherapy for solid tumors, typically 5 × 5 Gy and 3 × 8 Gy and total does of 20–30 Gy are applied.

The plasma concentrations of IFN-β and TNF-α at 6 h after the last administration were analyzed using ELISA kits. CPs-CDN and free CDN drastically promoted the secretion of IFN-β and TNF-α compared to PBS or 3 Gy X-ray (Fig. 5d). The combination of CPs-CDN or free CDN with 3 Gy X-ray further increased IFN-β expression (***p). Notably, 5 Gy X-ray significantly reenforced CPs-CDN to secrete abundant IFN-β and TNF-α (***p), accompanied with acute necrosis in tumors. The increase in plasma IFN-β levels by the combination of CPs-CDN and RT reflects an enhanced activation of STING pathway and better antitumor immune response. Type I IFNs (IFN-α and IFN-β) were shown to promote maturation and migration of DCs, enhance cytotoxicity mediated by $CD8^+$ T cells, and bridge innate and adaptive immunity, besides direct inhibitory effect on tumor cells [65,66]. It should be noted that under stimulation, multiple cells in tumor including DCs, tumor cells, macrophages, and T cells are capable of producing IFN-β *in vivo*. APCs were reported to induce the highest IFN-β production while much lower IFN-β production by B16F10 cells [34].

4. Conclusion

We have shown that polymersome-mediated cytosolic delivery of cyclic dinucleotide STING agonist (CPs-CDN) greatly enhances tumor immunotherapy and radioimmunotherapy via augmenting tumor retention, tumor draining lymph node uptake, dendritic cell uptake and maturation, and intracellular trafficking and release. Interestingly, in contrast to free ADU-S100 and 3 Gy X-ray that induce little tumor infiltration of CTLs, CPs-CDN leads to greatly increased CTLs in tumor microenvironment, illustrating a unique role of polymersome-mediated cytosolic delivery. The combination of CPs-CDN with 5 Gy X-ray further re-enforces STING activation, promotes the secretion of IFN-β and TNF-α, increases the proportions of mature DCs and effector T cells, and reduces immunosuppressive M2M in TME, yielding further enhanced and durable anti-tumor immune responses with significant survival benefits and cure of 3/7 B16F10-bearing mice. The reduction of systemic exposure of STING agonist enabled by polymersomes, on the other hand, might also alleviate their adverse effects. This polymersome-facilitated cytosolic delivery of STING agonists appears to be an attractive strategy to boost cancer immunotherapy. Besides local *i.t.* injection, polymersomal CDN might also be delivered systemically as reported for CpG and siRNA [37,44,45]. The dense PEGylation, neutral surface charge and favorable size of CPs-CDN facilitate effective bypass of phagocytosis [67,68]. This study has proven the concept that CPs-CDN can elegantly solve the issues of free CDNs such as fast clearance, poor cell uptake and inefficient cytosolic transportation and boost the immunotherapy of B16F10 melanoma mouse model. B16F10 melanoma is a typical model used for immunotherapeutic studies because it is highly malignant and immunogenic. Advanced metastatic melanoma remains highly challenging to treat in the clinics. In the future, we will further investigate the efficacy of CPs-CDN in more and clinically relevant models including denser solid tumors in which tumor penetration is another limiting factor.

Declaration of competing interest

The authors declare no known competing financial interest.

CRediT authorship contribution statement

Huan Zheng: Methodology, Investigation, Validation, Writing – original draft. **Beibei Guo:** Investigation, Data curation. **Xinyun Qiu:** Methodology, Investigation. **Yifeng Xia:** Investigation, Data curation. **Yan Qu:** Data curation. **Liang Cheng:** Resources, Visualization. **Fenghua Meng:** Conceptualization, Supervision, Writing – review & editing. **Zhiyuan Zhong:** Conceptualization, Supervision, Writing – review & editing.

Acknowledgements

This work is supported by research grants from the National Natural Science Foundation of China (NSFC 52033006, 51861145310, 51773146 and 51633005) and the National Key R&D Program of China (2021YFB3800900).

Appendix A. Supplementary data

Supplementary data to this article can be found online at https://doi.org/10.1016/j.bioactmat.2022.02.029.

References

[1] W. Wang, J. Jiang, C. Wu, CAR-NK for tumor immunotherapy: clinical transformation and future prospects, Cancer Lett. 472 (2020) 175–180, https://doi.org/10.1016/j.canlet.2019.11.033.

[2] J. Nam, S. Son, K.S. Park, W. Zou, L.D. Shea, J.J. Moon, Cancer nanomedicine for combination cancer immunotherapy, Nat. Rev. Mater. 4 (2019) 398–414, https://doi.org/10.1038/s41578-019-0108-1.

[3] J. Xu, J. Lv, Q. Zhuang, Z. Yang, Z. Cao, L. Xu, P. Pei, C. Wang, H. Wu, Z. Dong, Y. Chao, C. Wang, K. Yang, R. Peng, Y. Cheng, Z. Liu, A general strategy towards personalized nanovaccines based on fluoropolymers for post-surgical cancer immunotherapy, Nat. Nanotechnol. 15 (2020) 1043–1052, https://doi.org/10.1038/s41565-020-00781-4.

[4] F.S. Hodi, S.J. O'Day, D.F. McDermott, R.W. Weber, J.A. Sosman, J.B. Haanen, R. Gonzalez, C. Robert, D. Schadendorf, J.C. Hassel, W. Akerley, A.J. van den Eertwegh, J. Lutzky, P. Lorigan, J.M. Vaubel, G.P. Linette, D. Hogg, C. H. Ottensmeier, C. Lebbe, C. Peschel, I. Quirt, J.I. Clark, J.D. Wolchok, J.S. Weber, J. Tian, M.J. Yellin, G.M. Nichol, A. Hoos, W.J. Urba, Improved survival with Ipilimumab in patients with metastatic melanoma, N. Engl. J. Med. 363 (2010) 711–723, https://doi.org/10.1056/NEJMoa1003466.

[5] S.C. Formenti, N.-P. Rudqvist, E. Golden, B. Cooper, E. Wennerberg, C. Lhuillier, C. Vanpouille-Box, K. Friedman, L. Ferrari de Andrade, K.W. Wucherpfennig, A. Heguy, N. Imai, S. Gnjatic, R.O. Emerson, X.K. Zhou, T. Zhang, A. Chachoua, S. Demaria, Radiotherapy induces responses of lung cancer to CTLA-4 blockade, Nat. Med. 24 (2018) 1845–1851, https://doi.org/10.1038/s41591-018-0232-2.

[6] M. Duruisseaux, A. Martinez-Cardus, M.E. Calleja-Cervantes, S. Moran, M. Castro de Moura, V. Davalos, D. Pineyro, M. Sanchez-Cespedes, N. Girard, M. Brevet, E. Giroux-Leprieur, C. Dumenil, M. Pradotto, P. Bironzo, E. Capelletto, S. Novello, A. Cortot, M.C. Copin, N. Karachaliou, M. Gonzalez-Cao, S. Peralta, L. M. Montuenga, I. Gil-Bazo, I. Baraibar, M.D. Lozano, M. Varela, J.C. Ruffinelli, R. Palmero, E. Nadal, T. Moran, L. Perez, I. Ramos, Q. Xiao, A.F. Fernandez, M. F. Fraga, M. Gut, I. Gut, C. Teixido, N. Vilarino, A. Prat, N. Reguart, A. Benito, P. Garrido, I. Barragan, J.F. Emile, R. Rosell, E. Brambilla, M. Esteller, Epigenetic prediction of response to anti-PD-1 treatment in non-small-cell lung cancer: a multicentre, retrospective analysis, Lancet Respir. Med. 6 (2018) 771–781, https://doi.org/10.1016/S2213-2600(18)30284-4.

[7] J.A. Beaver, M. Hazarika, F. Mulkey, S. Mushti, H. Chen, K. He, R. Sridhara, K. B. Goldberg, M.K. Chuk, D.C. Chi, J. Chang, A. Barone, S. Balasubramaniam, G. M. Blumenthal, P. Keegan, R. Pazdur, M.R. Theoret, Patients with melanoma treated with an anti-PD-1 antibody beyond recist progression: a US food and drug administration pooled analysis, Lancet Oncol. 19 (2018) 229–239, https://doi.org/10.1016/S1470-2045(17)30846-X.

[8] J. Xu, Y. Zhang, R. Jia, C. Yue, L. Chang, R. Liu, G. Zhang, C. Zhao, Y. Zhang, C. Chen, Y. Wang, X. Yi, Z. Hu, J. Zou, Q. Wang, Anti-PD-1 antibody SHR-1210 combined with Apatinib for advanced hepatocellular carcinoma, gastric, or esophagogastric junction cancer: an open-label, dose escalation and expansion study, Clin. Cancer Res. 25 (2019) 515–523, https://doi.org/10.1158/1078-0432.CCR-18-2484.

[9] M. Kowanetz, W. Zou, S.N. Gettinger, H. Koeppen, M. Kockx, P. Schmid, E.E. Kadel, I. Wistuba, J. Chaft, N.A. Rizvi, D.R. Spigel, A. Spira, F.R. Hirsch, V. Cohen, D. Smith, Z. Boyd, N. Miley, S. Flynn, V. Leveque, D.S. Shames, M. Ballinger, S. Mocci, G. Shankar, R. Funke, G. Hampton, A. Sandler, L. Amler, I. Mellman, D. S. Chen, P.S. Hegde, Differential regulation of PD-L1 expression by immune and tumor cells in NSCLC and the response to treatment with atezolizumab (anti–PD-L1), Proc. Natl. Acad. Sci. U. S. A. 115 (2018) E10119–E10126, https://doi.org/10.1073/pnas.1802166115.

[10] L.A. Emens, C. Cruz, J.P. Eder, F. Braiteh, C. Chung, S.M. Tolaney, I. Kuter, R. Nanda, P.A. Cassier, J.P. Delord, M.S. Gordon, E. ElGabry, C.W. Chang, I. Sarkar, W. Grossman, C. O'Hear, M. Fassò, L. Molinero, P. Schmid, Long-term clinical outcomes and biomarker analyses of Atezolizumab therapy for patients with metastatic triple-negative breast cancer: a phase 1 study, JAMA Oncol. 5 (2019) 74–82, https://doi.org/10.1001/jamaoncol.2018.4224.

[11] A. Sharma, S.K. Subudhi, J. Blando, J. Scutti, L. Vence, J. Wargo, J.P. Allison, A. Ribas, P. Sharma, Anti-CTLA-4 immunotherapy does not deplete FoxP3(+) regulatory T cells (Tregs) in human cancers, Clin. Cancer Res. 25 (2019) 1233–1238, https://doi.org/10.1158/1078-0432.CCR-18-0762.

[12] Y. Sabet, S. Ramirez, E. Rosell Cespedes, M. Rensoli Velasquez, M. Porres-Muñoz, S. Gaur, J.B. Figueroa-Casas, M. Porres-Aguilar, Severe acute pulmonary toxicity associated with brentuximab in a patient with refractory hodgkin's lymphoma, Case Rep. Pulmonol. 2016 (2016), 2359437, https://doi.org/10.1155/2016/2359437.

[13] A. Younes, A. Santoro, M. Shipp, P.L. Zinzani, J.M. Timmerman, S. Ansell, P. Armand, M. Fanale, V. Ratanatharathorn, J. Kuruvilla, J.B. Cohen, G. Collins, K. J. Savage, M. Trneny, K. Kato, B. Farsaci, S.M. Parker, S. Rodig, M.G.M. Roemer, A. H. Ligon, A. Engert, Nivolumab for classical Hodgkin's lymphoma after failure of both autologous stem-cell transplantation and brentuximab vedotin: a multicentre, multicohort, single-arm phase 2 trial, Lancet Oncol. 17 (2016) 1283–1294, https://doi.org/10.1016/S1470-2045(16)30167-X.

[14] M. Collins, W. Kong, I. Jung, M. Wang, S.M. Lundh, C.H. June, J.J. Melenhorst, A failure to start: aborted activation of CAR T cells in chronic lymphocytic leukemia, Blood 134 (2019), 681, https://doi.org/10.1182/blood-2019-122063.

[15] D. Mahony, J.C. Morris, C. Quinn, W. Gao, W.H. Wilson, B. Gause, S. Pittaluga, S. Neelapu, M. Brown, T.A. Fleisher, J.L. Gulley, J. Schlom, R. Nussenblatt, P. Albert, T.A. Davis, I. Lowy, M. Petrus, T.A. Waldmann, J.E. Janik, A pilot study of CTLA-4 blockade after cancer vaccine failure in patients with advanced malignancy, Clin. Cancer Res. 13 (2007) 958–964, https://doi.org/10.1158/1078-0432.CCR-06-1974.

[16] J.E. Kim, M.A. Patel, A. Mangraviti, E.S. Kim, D. Theodros, E. Velarde, A. Liu, E. W. Sankey, A. Tam, H. Xu, D. Mathios, C.M. Jackson, S. Harris-Bookman, T. Garzon-Muvdi, M. Sheu, A.M. Martin, B.M. Tyler, P.T. Tran, X. Ye, A. Olivi, J. M. Taube, P.C. Burger, C.G. Drake, H. Brem, D.M. Pardoll, M. Lim, Combination therapy with anti-PD-1, anti-TIM-3, and focal radiation results in regression of murine gliomas, Clin. Cancer Res. 23 (2017) 124–136, https://doi.org/10.1158/1078-0432.CCR-15-1535.

[17] M.Z. Dewan, A.E. Galloway, N. Kawashima, J.K. Dewyngaert, J.S. Babb, S. C. Formenti, S. Demaria, Fractionated but not single-dose radiotherapy induces an immune-mediated abscopal effect when combined with anti–CTLA-4 antibody, Clin. Cancer Res. 15 (2009) 5379–5388, https://doi.org/10.1158/1078-0432.CCR-09-0265.

[18] J. Nie, C. Wang, Y. Liu, Q. Yang, Q. Mei, L. Dong, X. Li, J. Liu, W. Ku, Y. Zhang, M. Chen, X. An, L. Shi, M.V. Brock, J. Bai, W. Han, Addition of low-dose decitabine to anti–PD-1 antibody camrelizumab in relapsed/refractory classical Hodgkin lymphoma, J. Clin. Oncol. 37 (2019) 1479–1489, https://doi.org/10.1200/JCO.18.02151.

[19] C. Wang, L. Xu, C. Liang, J. Xiang, R. Peng, Z. Liu, Immunological responses triggered by photothermal therapy with carbon nanotubes in combination with anti-CTLA-4 therapy to inhibit cancer metastasis, Adv. Mater. 26 (2014) 8154–8162, https://doi.org/10.1002/adma.201402996.

[20] L. Corrales, S.M. McWhirter, T.W. Dubensky Jr., T.F. Gajewski, The host STING pathway at the interface of cancer and immunity, J. Clin. Invest. 126 (2016) 2404–2411, https://doi.org/10.1172/JCI86892.

[21] T. Su, Y. Zhang, K. Valerie, X.Y. Wang, S. Lin, G. Zhu, STING activation in cancer immunotherapy, Theranostics 9 (2019) 7759–7771, https://doi.org/10.7150/thno.37574.

[22] L. Corrales, Laura H. Glickman, Sarah M. McWhirter, David B. Kanne, Kelsey E. Sivick, George E. Katibah, S.-R. Woo, E. Lemmens, T. Banda, Justin J. Leong, K. Metchette, Thomas W. Dubensky, Thomas F. Gajewski, Direct activation of STING in the tumor microenvironment leads to potent and systemic tumor regression and immunity, Cell Rep. 11 (2015) 1018–1030, https://doi.org/10.1016/j.celrep.2015.04.031.

[23] J.B. Foote, M. Kok, J.M. Leatherman, T.D. Armstrong, B.C. Marcinkowski, L. S. Ojalvo, D.B. Kanne, E.M. Jaffee, T.W. Dubensky Jr., L.A. Emens, A STING agonist given with OX40 receptor and PD-L1 modulators primes immunity and reduces tumor growth in tolerized mice, Cancer Immunol. Res. 5 (2017) 468–479, https://doi.org/10.1158/2326-6066.CIR-16-0284.

[24] K.E. Sivick, A.L. Desbien, L.H. Glickman, G.L. Reiner, L. Corrales, N.H. Surh, T. E. Hudson, U.T. Vu, B.J. Francica, T. Banda, G.E. Katibah, D.B. Kanne, J.J. Leong, K. Metchette, J.R. Bruml, C.O. Ndubaku, J.M. McKenna, Y. Feng, L. Zheng, S. L. Bender, C.Y. Cho, M.L. Leong, A. van Elsas, T.W. Dubensky, S.M. McWhirter, Magnitude of therapeutic STING activation determines CD8+ T cell-mediated anti-tumor immunity, Cell Rep. 29 (2019) 785–789, https://doi.org/10.1016/j.celrep.2019.09.089.

[25] R.D. Junkins, M.D. Gallovic, B.M. Johnson, M.A. Collier, R. Watkins-Schulz, N. Cheng, C.N. David, C.E. McGee, G.D. Sempowski, I. Shterev, K. McKinnon, E. M. Bachelder, K.M. Ainslie, J.P.Y. Ting, A robust microparticle platform for a STING-targeted adjuvant that enhances both humoral and cellular immunity during vaccination, J. Contr. Release 270 (2018) 1–13, https://doi.org/10.1016/j.jconrel.2017.11.030.

[26] A. Amouzegar, M. Chelvanambi, J.N. Filderman, W.J. Storkus, J.J. Luke, STING agonists as cancer therapeutics, Cancers 13 (2021) 1–24, https://doi.org/10.3390/cancers13112695.

[27] D.G. Leach, N. Dharmaraj, S.L. Piotrowski, T.L. Lopez-Silva, Y.L. Lei, A.G. Sikora, S. Young, J.D. Hartgerink, STINGel: controlled release of a cyclic dinucleotide for enhanced cancer immunotherapy, Biomaterials 163 (2018) 67–75, https://doi.org/10.1016/j.biomaterials.2018.01.035.

[28] N.M. Munoz, M. Williams, K. Dixon, C. Dupuis, A. McWatters, R. Avritscher, S. Z. Manrique, K. McHugh, R. Murthy, A. Tam, A. Naing, S.P. Patel, D. Leach, J. D. Hartgerink, S. Young, P. Prakash, P. Hwu, R.A. Sheth, Influence of injection technique, drug formulation and tumor microenvironment on intratumoral immunotherapy delivery and efficacy, J. Immunother. Cancer 9 (2021), e001800, https://doi.org/10.1136/jitc-2020-001800.

[29] X.G. Lu, W.T. Gao, Z.Q. Chen, K.J. McHugh, Y.H. Sun, Z. Tochka, S. Tomasic, K. Sadtler, A. Hyacinthe, Y.X. Huang, T. Graf, Q.Y Hu, M. Sarmadi, R. Langer, D. G. Anderson, A. Jaklenec, Engineered PLGA microparticles for long-term, pulsatile release of STING agonist for cancer immunotherapy, Sci. Transl. Med. 12 (2020), eaaz6606, https://doi.org/10.1126/scitranslmed.aaz6606.

[30] M. An, C. Yu, J. Xi, J. Reyes, G. Mao, W.-Z. Wei, H. Liu, Induction of necrotic cell death and activation of STING in the tumor microenvironment via cationic silica nanoparticles leading to enhanced antitumor immunity, Nanoscale 10 (2018) 9311–9319, https://doi.org/10.1039/c8nr01376d.

[31] S.T. Koshy, A.S. Cheung, L. Gu, A.R. Graveline, D.J. Mooney, Liposomal delivery enhances immune activation by STING agonists for cancer immunotherapy, Adv. Biosyst 1 (2017), 1600013, https://doi.org/10.1002/adbi.201600013.

[32] N. Cheng, R. Watkins-Schulz, R.D. Junkins, C.N. David, B.M. Johnson, S. A. Montgomery, K.J. Peine, D.B. Darr, H. Yuan, K.P. McKinnon, Q. Liu, L. Miao, L. Huang, E.M. Bachelder, K.M. Ainslie, J.P. Ting, A nanoparticle-incorporated STING activator enhances antitumor immunity in PD-L1-insensitive models of triple-negative breast cancer, JCI Insight 3 (2018) 3–20, https://doi.org/10.1172/jci.insight.120638.

[33] M. Wehbe, L. Wang-Bishop, K.W. Becker, D. Shae, J.J. Baljon, X. He, P. Christov, K. L. Boyd, J.M. Balko, J.T. Wilson, Nanoparticle delivery improves the pharmacokinetic properties of cyclic dinucleotide STING agonists to open a therapeutic window for intravenous administration, J. Contr. Release 330 (2021) 1118–1129, https://doi.org/10.1016/j.jconrel.2020.11.017.

[34] D. Shae, K.W. Becker, P. Christov, D.S. Yun, A.K.R. Lytton-Jean, S. Sevimli, M. Ascano, M. Kelley, D.B. Johnson, J.M. Balko, J.T. Wilson, Endosomolytic polymersomes increase the activity of cyclic dinucleotide STING agonists to enhance cancer immunotherapy, Nat. Nanotechnol. 14 (2019) 269–278, https://doi.org/10.1038/s41565-018-0342-5.

[35] Y. Jiang, W. Yang, J. Zhang, F. Meng, Z. Zhong, Protein toxin chaperoned by LRP-1-targeted virus-mimicking vesicles induces high-efficiency glioblastoma therapy in vivo, Adv. Mater. 30 (2018), e1800316, https://doi.org/10.1002/adma.201800316.

[36] W. Yang, Y. Wei, L. Yang, J. Zhang, Z. Zhong, G. Storm, F. Meng, Granzyme B-loaded, cell-selective penetrating and reduction-responsive polymersomes effectively inhibit progression of orthotopic human lung tumor in vivo, J. Contr. Release 290 (2018) 141–149, https://doi.org/10.1016/j.jconrel.2018.10.013.

[37] Y. Zou, M. Zheng, W. Yang, F. Meng, K. Miyata, H.J. Kim, K. Kataoka, Z. Zhong, Virus-mimicking chimaeric polymersomes boost targeted cancer siRNA therapy in vivo, Adv. Mater. 29 (2017), 1703285, https://doi.org/10.1002/adma.201703285.

[38] C. Lhuillier, N.P. Rudqvist, O. Elemento, S.C. Formenti, S. Demaria, Radiation therapy and anti-tumor immunity: exposing immunogenic mutations to the immune system, Genome Med. 11 (2019) 2–10, https://doi.org/10.1186/s13073-019-0653-7.

[39] L. Galluzzi, A. Buqué, O. Kepp, L. Zitvogel, G. Kroemer, Immunogenic cell death in cancer and infectious disease, Nat. Rev. Immunol. 17 (2016) 97–111, https://doi.org/10.1038/nri.2016.107.

[40] M. Uribe-Herranz, S. Rafail, S. Beghi, L. Gil-de-Gomez, I. Verginadis, K. Bittinger, S. Pustylnikov, S. Pierini, R. Perales-Linares, I.A. Blair, C.A. Mesaros, N.W. Snyder, F. Bushman, C. Koumenis, A. Facciabene, Gut microbiota modulate dendritic cell antigen presentation and radiotherapy-induced antitumor immune response, J. Clin. Invest. 130 (2020) 466–479, https://doi.org/10.1172/JCI124332.

[41] L. Deng, H. Liang, S. Fu, R.R. Weichselbaum, Y.X. Fu, From DNA damage to nucleic acid sensing: a strategy to enhance radiation therapy, Clin. Cancer Res. 22 (2016) 20–25, https://doi.org/10.1158/1078-0432.CCR-14-3110.

[42] A. Mullard, Can innate immune system targets turn up the heat on 'cold' tumours? Nat. Rev. Drug Discov. 17 (2018) 3–5, https://doi.org/10.1038/nrd.2017.264.

[43] S. Vrignaud, J.P. Benoit, P. Saulnier, Strategies for the nanoencapsulation of hydrophilic molecules in polymer-based nanoparticles, Biomaterials 32 (2011) 8593–8604, https://doi.org/10.1016/j.biomaterials.2011.07.057.

[44] Y. Shi, Y. Jiang, J. Cao, W. Yang, J. Zhang, F. Meng, Z. Zhong, Boosting RNAi therapy for orthotopic glioblastoma with nontoxic brain-targeting chimaeric polymersomes, J. Contr. Release 292 (2018) 163–171, https://doi.org/10.1016/j.jconrel.2018.10.034.

[45] Y. Xia, J. Wei, S. Zhao, B. Guo, F. Meng, B. Klumperman, Z. Zhong, Systemic administration of polymersomal oncolytic peptide LTX-315 combining with CPG adjuvant and anti-PD-1 antibody boosts immunotherapy of melanoma, J. Contr. Release 336 (2021) 262–273, https://doi.org/10.1016/j.jconrel.2021.06.032.

[46] E. Lee, H.E. Jang, Y.Y. Kang, J. Kim, J.H. Ahn, H. Mok, Submicron-sized hydrogels incorporating cyclic dinucleotides for selective delivery and elevated cytokine

release in macrophages, Acta Biomater. 29 (2016) 271–281, https://doi.org/10.1016/j.actbio.2015.10.025.
[47] J.R. Baird, D. Friedman, B. Cottam, T.W. Dubensky Jr., D.B. Kanne, S. Bambina, K. Bahjat, M.R. Crittenden, M.J. Gough, Radiotherapy combined with novel STING-targeting oligonucleotides results in regression of established tumors, Cancer Res. 76 (2016) 50–61, https://doi.org/10.1158/0008-5472.CAN-14-3619.
[48] H. Wang, S. Hu, X. Chen, H. Shi, C. Chen, L. Sun, Z.J. Chen, cGAS is essential for the antitumor effect of immune checkpoint blockade, P. Natl. Acad. Sci. USA 114 (2017) 1637–1642, https://doi.org/10.1073/pnas.1621363114.
[49] M. Motwani, S. Pesiridis, K.A. Fitzgerald, DNA sensing by the cGAS–STING pathway in health and disease, Nat. Rev. Genet. 20 (2019) 657–674, https://doi.org/10.1038/s41576-019-0151-1.
[50] F. Veglia, D.I. Gabrilovich, Dendritic cells in cancer: the role revisited, Curr. Opin. Immunol. 45 (2017) 43–51, https://doi.org/10.1016/j.coi.2017.01.002.
[51] Y. Liu, X. Cao, Intratumoral dendritic cells in the anti-tumor immune response, Cell. Mol. Immunol. 12 (2015) 387–390, https://doi.org/10.1038/cmi.2014.130.
[52] A.W. Li, M.C. Sobral, S. Badrinath, Y. Choi, A. Graveline, A.G. Stafford, J. C. Weaver, M.O. Dellacherie, T.-Y. Shih, O.A. Ali, J. Kim, K.W. Wucherpfennig, D. J. Mooney, A facile approach to enhance antigen response for personalized cancer vaccination, Nat. Mater. 17 (2018) 528–534, https://doi.org/10.1038/s41563-018-0028-2.
[53] W. Yang, Z. Zhou, J. Lau, S. Hu, X. Chen, Functional T cell activation by smart nanosystems for effective cancer immunotherapy, Nano, Today Off. 27 (2019) 28–47, https://doi.org/10.1016/j.nantod.2019.05.004.
[54] B.A. Flood, E.F. Higgs, S. Li, J.J. Luke, T.F. Gajewski, STING pathway agonism as a cancer therapeutic, Immunol. Rev. 290 (2019) 24–38, https://doi.org/10.1111/imr.12765.
[55] T. Li, Z.J. Chen, The cGAS-cGAMP-STING pathway connects DNA damage to inflammation, senescence, and cancer, J. Exp. Med. 215 (2018) 1287–1299, https://doi.org/10.1084/jem.20180139.
[56] G. Shang, C. Zhang, Z.J. Chen, X.C. Bai, X. Zhang, Cryo-em structures of STING reveal its mechanism of activation by cyclic GMP-AMP, Nature 567 (2019) 389–393, https://doi.org/10.1038/s41586-019-0998-5.
[57] H. Cabral, Y. Matsumoto, K. Mizuno, Q. Chen, M. Murakami, M. Kimura, Y. Terada, M.R. Kano, K. Miyazono, M. Uesaka, N. Nishiyama, K. Kataoka, Accumulation of sub-100 nm polymeric micelles in poorly permeable tumours depends on size, Nat. Nanotechnol. 6 (2011) 815–823, https://doi.org/10.1038/nnano.2011.166.
[58] Z. Zhang, H. Wang, T. Tan, J. Li, Z. Wang, Y. Li, Rational design of nanoparticles with deep tumor penetration for effective treatment of tumor metastasis, Adv. Funct. Mater. 28 (2018), 1801840, https://doi.org/10.1002/adfm.201801840.
[59] J. Ahn, T. Xia, A. Rabasa Capote, D. Betancourt, G.N. Barber, Extrinsic phagocyte-dependent STING signaling dictates the immunogenicity of dying cells, Cancer Cell 33 (2018) 862–873, https://doi.org/10.1016/j.ccell.2018.03.027.
[60] M.M. Ahmed, A. Narendra, P. Prasanna, C.N. Coleman, S. Krishnan, Current insights in radiation combination therapies: influence of omics and novel targeted agents in defining new concepts in radiation biology and clinical radiation oncology, Semin. Radiat. Oncol. 26 (2016) 251–253, https://doi.org/10.1016/j.semradonc.2016.07.002.
[61] Y. Liu, W.N. Crowe, L. Wang, Y. Lu, W.J. Petty, A.A. Habib, D. Zhao, An inhalable nanoparticulate STING agonist synergizes with radiotherapy to confer long-term control of lung metastases, Nat. Commun. 10 (2019), 5108, https://doi.org/10.1038/s41467-019-13094-5.
[62] L. Deng, H. Liang, M. Xu, X. Yang, B. Burnette, A. Arina, X.D. Li, H. Mauceri, M. Beckett, T. Darga, X. Huang, T.F. Gajewski, Z.J. Chen, Y.X. Fu, R. R. Weichselbaum, STING-dependent cytosolic DNA sensing promotes radiation-induced type I interferon-dependent antitumor immunity in immunogenic tumors, Immunity 41 (2014) 843–852, https://doi.org/10.1016/j.immuni.2014.10.019.
[63] A. Schudel, D.M. Francis, S.N. Thomas, Material design for lymph node drug delivery, Nat. Rev. Mater. 4 (2019) 415–428, https://doi.org/10.1038/s41578-019-0110-7.
[64] M.C. Chang, Y.L. Chen, H.W. Lin, Y.C. Chiang, C.F. Chang, S.F. Hsieh, C.A. Chen, W.Z. Sun, W.F. Cheng, Irradiation enhances abscopal anti-tumor effects of antigen-specific immunotherapy through regulating tumor microenvironment, Mol. Ther. 26 (2018) 404–419, https://doi.org/10.1016/j.ymthe.2017.11.011.
[65] A. Li, M. Yi, S. Qin, Y. Song, Q. Chu, K. Wu, Activating cGAS-STING pathway for the optimal effect of cancer immunotherapy, J. Hematol. Oncol. 12 (2019), 35, https://doi.org/10.1186/s13045-019-0721-x.
[66] L.M. Snell, T.L. McGaha, D.G. Brooks, Type I interferon in chronic virus infection and cancer, Trends Immunol. 38 (2017) 542–557, https://doi.org/10.1016/j.it.2017.05.005.
[67] M.J. Mitchell, M.M. Billingsley, R.M. Haley, M.E. Wechsler, N.A. Peppas, R. Langer, Engineering precision nanoparticles for drug delivery, Nat. Rev. Drug Discov. 20 (2021) 101–124, https://doi.org/10.1038/s41573-020-0090-8.
[68] J. Ding, J. Chen, L. Gao, Z. Jiang, Y. Zhang, M. Li, Q. Xiao, S.S. Lee, X. Chen, Engineered nanomedicines with enhanced tumor penetration, Nano Today 29 (2019), 100800, https://doi.org/10.1016/j.nantod.2019.100800.